



## OPEN

# A30P $\alpha$ -Synuclein interferes with the stable integration of adult-born neurons into the olfactory network

SUBJECT AREAS:  
OLFACTORY BULB  
PARKINSON'S DISEASE  
ADULT NEUROGENESIS  
TECHNICAL REPORT

Johanna Neuner<sup>1</sup>, Severin Filser<sup>2</sup>, Stylianos Michalakis<sup>3</sup>, Martin Biel<sup>3</sup> & Jochen Herms<sup>2,4</sup>

Received  
8 April 2013

Accepted  
6 January 2014

Published  
3 February 2014

Correspondence and requests for materials should be addressed to J.H. (jochen.herms@med.uni-muenchen.de)

<sup>1</sup>Center for Neuropathology and Prion Research, Ludwig Maximilian University Munich, Feodor-Lynen-Straße 23, 81377 Munich, Germany, <sup>2</sup>German Center for Neurodegenerative Diseases (DZNE), Munich, Schillerstraße 44, 80336 Munich, Germany, <sup>3</sup>Center for Integrated Protein Science Munich, CIPSM and Department of Pharmacy-Center for Drug Research, Ludwig Maximilian University Munich, Butenandtstr. 5-13, 81377 Munich, Germany, <sup>4</sup>Munich Cluster of Systems Neurology (SyNergy), Ludwig Maximilian University Munich, Schillerstraße 44, 80336 Munich, Germany.

Impaired olfaction is an early symptom in Parkinson disease (PD), although the exact cause is as yet unknown. Here, we investigated the link between PD-related mutant  $\alpha$ -Synuclein ( $\alpha$ -SYN) pathology and olfactory deficit, by examining the integration of adult-born neurons in the olfactory bulb (OB) of A30P  $\alpha$ -SYN overexpressing mice. To this end, we chose to label one well-known vulnerable subpopulation of adult-born cells, the dopaminergic neurons. Using *in vivo* two-photon imaging, we followed the dynamic process of neuronal turnover in transgenic A30P  $\alpha$ -SYN and wild-type mice over a period of 2.5 months. Our results reveal no difference in the number of cells that reach, and possibly integrate into, the glomerular layer in the OB. However, in mutant transgenic mice these new neurons have a significantly shortened survival, resulting in an overall reduction in the addition of neurons to the glomerular layer over time. We therefore propose unstable integration and impaired homeostasis of functional new neurons as a likely contributor to odour discrimination deficits in mutant  $\alpha$ -SYN mice.

H yposmia is one of the most frequent non-motor symptoms of Parkinson disease (PD)<sup>1–3</sup>, being detected in the majority of PD patients several years before the first appearance of motor symptoms<sup>4</sup>. Moreover, deposition of fibrillar  $\alpha$ -synuclein ( $\alpha$ -SYN) aggregates<sup>5,6</sup> - the main pathological hallmark of the disease - occurs inside olfactory bulb (OB) neurons of PD patients<sup>7,8</sup>. Despite evidence of olfactory deficits in  $\alpha$ -SYN overexpressing mice<sup>9</sup>, no satisfactory explanation has yet been put forward which correlates the neuropathological findings with the behavioural deficit. Interestingly, a deficit of neuronal precursor cells was discovered in the OB of PD patients compared with healthy controls<sup>10</sup>. Studies in mice further linked  $\alpha$ -SYN overexpression to reduced survival of adult-born OB neurons<sup>11–14</sup>, including both periglomerular neurons (PGNs) and granule cells (GCs). Despite the evidence gained from these studies, we still lack a thorough investigation of the long-term effects of  $\alpha$ -SYN aggregates on this highly dynamic process of neuronal turnover which occurs in the OB<sup>15</sup>. Undoubtedly, continuous incorporation of 'virgin' neurons into pre-existing networks poses a considerable physiological challenge, since their survival depends very much on the activity of local circuits and extrinsic influences<sup>16–20</sup>. Functional synaptic plasticity and integration requires communication with network neurons at the integration site and is a prerequisite for their contribution to olfactory circuits<sup>21–23</sup>. For instance, by synapsing with mitral cells (MCs), adult-born neurons sharpen odour tuning and provide contrast enhancement, important determinants for odour discrimination<sup>24,25</sup>. It is thus not surprising that this complex, fine-tuned, turnover of gained-and-lost neurons is closely coupled with olfactory stimulation<sup>22</sup>. Thus, odour deprivation decreases the number of new neurons in the OB<sup>19</sup>, whereas odour enrichment promotes their survival<sup>20</sup>.

In our study, we aimed at correlating PD-related  $\alpha$ -SYN pathology in the OB network with olfactory deficits and the fate of adult-born neurons. To this end, we investigated in detail the  $\alpha$ -SYN pathology in the OB of A30P  $\alpha$ -SYN mice<sup>26</sup> and its impact on olfaction. Using chronic intravital two-photon imaging, we followed the turnover of adult-born neurons in the OB of transgenic  $\alpha$ -SYN and wild-type mice over a period of 2.5 months. We focused on dopaminergic PGNs as a subset of adult-born neurons, because (i) these are known to be primarily affected in PD<sup>27,28</sup>, (ii) they can be selectively labeled, and (iii) they have a superficial location thus making them accessible to two-photon imaging.



Herein, we report that aggregation-prone A30P  $\alpha$ -SYN interferes with the stable integration and longer-term survival of adult-born neurons, with possible consequences on odour discrimination.

## Results

**A30P  $\alpha$ -SYN mice are impaired in fine odour discrimination.** For the initial characterization of PD-related pathology, we examined  $\alpha$ -SYN aggregation in the OB of 6-month-old mice overexpressing human A30P  $\alpha$ -SYN under the Thy1-promoter<sup>26</sup>. The A30P mutation is known to cause severe, early-onset familial PD, accelerating the formation of toxic protein protofibrils<sup>29,30</sup>. Immunofluorescent staining with human  $\alpha$ -SYN-specific antibody 15G7<sup>31</sup> revealed broad protein expression throughout the OB network including its three main cell layers: glomerular, MC and GC layer (Fig. 1a). In comparison to mice with elevated  $\alpha$ -SYN levels in neuroblasts and immature newborn cells (PDGF $\beta$ -promoter)<sup>11,12</sup>, protein expression under neuron-specific Thy1<sup>26,32</sup> starts relatively late, thus providing a

suitable model for the study of neuronal integration and fate in  $\alpha$ -SYN-loaded networks in early-stage PD<sup>33</sup>.

In PD,  $\alpha$ -SYN is post-translationally modified (glycated, nitrated, oxidized or phosphorylated) and thereby more prone to forming aggregates and fibrils<sup>34</sup>. Thus, we characterized one form of pathological protein alteration by staining against phosphorylated  $\alpha$ -SYN, a major component of Lewy bodies (LB) in the human brain<sup>35</sup>. In transgenic, but not wild-type, mice phosphorylated  $\alpha$ -SYN was detected in the wide majority of MCs (Fig. 1b,d), while the glomerular (Fig. 1c) and GC layers (Fig. 1e) were largely spared<sup>36</sup>. In addition,  $\alpha$ -SYN was characterized by its resistance to proteinase K (PK) digestion, a property shared in common with fibrillar amyloid- $\beta$ , the major component of Alzheimer disease-related amyloid plaques, and with the disease-associated form of prion protein<sup>5</sup>.  $\alpha$ -SYN clusters were detected in some MCs of the transgenic mice (Fig. 1f,h) but were absent from wild-type mice. Rarely, we detected subcellular  $\alpha$ -SYN accumulations in the glomerular (Fig. 1g) and GC layer (Fig. 1i) of mutant  $\alpha$ -SYN mice. These findings in Thy1-A30P  $\alpha$ -

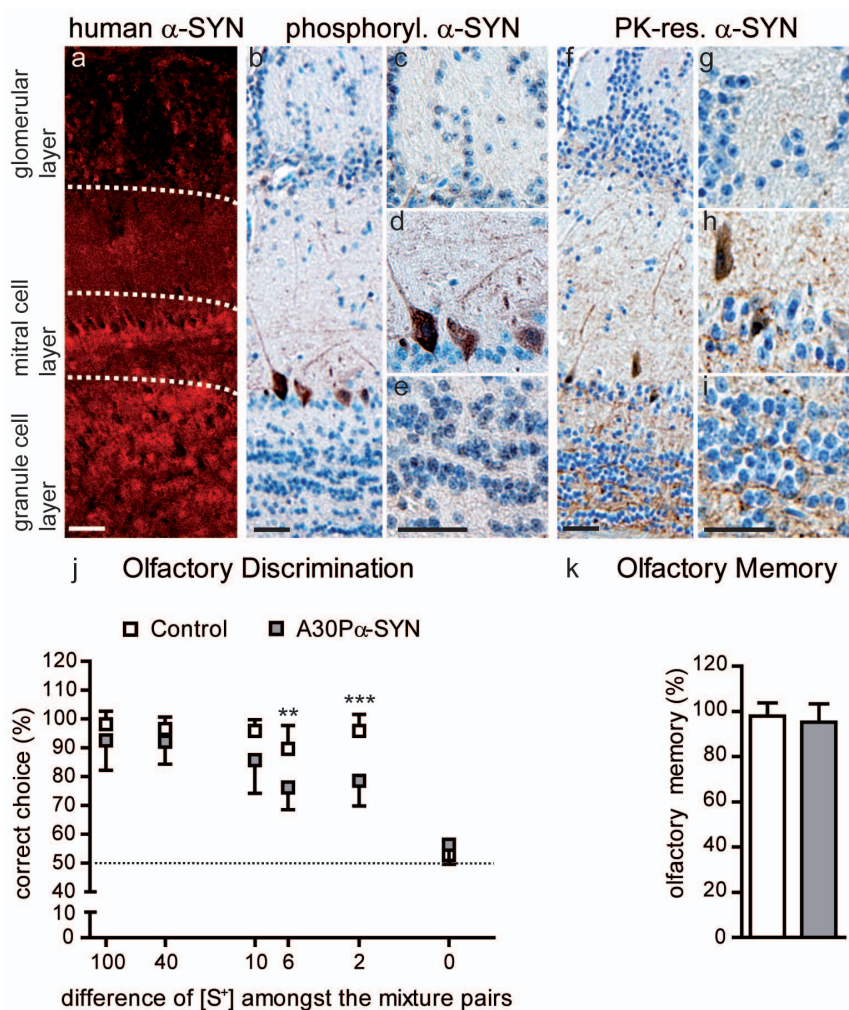


**Figure 1 | Olfactory bulb pathology in A30P  $\alpha$ -SYN mice.** (a) Immunofluorescent micrographs showing the overexpression pattern of human A30P  $\alpha$ -SYN (15G7, red) under control of the Thy1-promoter in the OB of 6-month-old transgenic mice: z-stack projections of confocal series. Scale bar - 50  $\mu$ m. (b–e) Representative OB sections immunostained for phosphorylated  $\alpha$ -SYN (pSer129, DAB), a marker for aberrant protein modification. Scale bars - 50  $\mu$ m. (b) Distribution of phosphorylated  $\alpha$ -SYN in (c) PGNs, (d) MCs and (e) GCs. Note that only MCs are positive for pSer129. (f–j) Representative OB sections with immunostaining for fibrillar protein, detected by Proteinase K digestion and human  $\alpha$ -SYN specific antibody (15G7, DAB). Scale bars - 50  $\mu$ m. Images with higher magnification of the (g) glomerular, (h) MC and (i) GC layer. Some  $\alpha$ -SYN aggregates were detected in MCs of transgenic, but not wild-type, mice. (j) Olfactory discrimination task. Six-month-old Control (wild-type) ( $n = 8$ ) and A30P  $\alpha$ -SYN mice ( $n = 7$ ) were exposed to different binary odour mixtures (e.g. 55% S<sup>+</sup> and 45% S<sup>-</sup> vs. 45% S<sup>+</sup> and 55% S<sup>-</sup>). Mice were trained to dig in a bowl containing more of S<sup>+</sup> odour. Correct choices for S<sup>+</sup> were plotted against the different mixture pairs. Note that with increasing similarity of the mixtures, the performance of A30P  $\alpha$ -SYN mice dropped compared to Control. (k) Olfactory memory task. \*\* $p < 0.01$ ; \*\*\* $p < 0.005$ ; two-way ANOVA/Bonferroni post-hoc test.



SYN mice thus reflect in part the neuropathology in the human PD brain, showing LBs in MCs and the inner plexiform layer<sup>7</sup>.

We further tested whether  $\alpha$ -SYN accumulation in the OB is associated with olfactory deficits in the transgenic mice. To this end, we used a simple battery test<sup>37,38</sup> which allows the detection of subtle differences in olfactory discrimination. Mice had to choose between increasingly similar solutions consisting of a mixture of two different odours (conditioned  $S^+$ ;  $S^-$ ), down to concentration differences of only 2% (Fig. 1j). Up to a 10% difference (55%  $S^+$  and 45%  $S^-$ ; *vice versa*), A30P  $\alpha$ -SYN mice performed just as wild-type Control. However, at mixtures with 6% difference (53%  $S^+$  and 47%  $S^-$ ; *vice versa*) the performance of PD-like mice dropped significantly when compared to Control ( $75 \pm 8\%$ ,  $n = 7$  mice vs.  $89 \pm 8\%$ ,  $n = 8$  mice, respectively;  $p < 0.01$ ). This discrepancy between the two genotypes grew markedly with the next difficulty step. Whereas wild-type mice managed to discriminate 2% different odour mixtures (51%  $S^+$  and 49%  $S^-$ ; *vice versa*) in 93  $\pm$  8% of the trials,  $\alpha$ -SYN mice succeeded in only 79  $\pm$  9% ( $p < 0.001$ ). As expected, 50% binary mixtures could not be distinguished by either group, with correct choices being close to the chance level of 50% (i.e. random). Importantly, during training and conditioning,  $\alpha$ -SYN and Control mice behaved and learned equally to discriminate  $S^+$  from  $S^-$  (average success rate of 90  $\pm$  8%, respectively;  $p > 0.05$ ). These results therefore indicate that 6 month-old A30P  $\alpha$ -SYN mice are impaired in fine, but not in pure and general odour discrimination. To test for effects of  $\alpha$ -SYN on olfactory long-term memory<sup>22</sup>, we confronted the mice with the different odours again after 2 months (Fig. 1k). Both genotypes recalled the test in the same way, showing that olfactory memory was not adversely affected by aggregation-prone A30P  $\alpha$ -SYN.

**Adult-born dopaminergic neurons are vulnerable to A30P  $\alpha$ -SYN deposition.** As an important aim of our study, we investigated the impact of A30P  $\alpha$ -SYN accumulation on the dynamic integration process of adult-born neurons. Due to their superficial location in the OB and their particular role in PD<sup>27,28</sup>, we chose one subset of adult-born neurons: dopaminergic PGNs, which constitute ~20–40% of all GABAergic PGNs<sup>39–41</sup>. In the glomerular layer of the transgenic  $\alpha$ -SYN mice, A30P  $\alpha$ -SYN was enriched in both tyrosine hydroxylase (TH)-positive dopaminergic neurons and other PGN subtypes (Fig. 2a). Notably, A30P  $\alpha$ -SYN had a significant impact on the density of TH-positive PGNs in both 6- (~30%;  $16,000 \pm 1,700$  vs.  $23,000 \pm 1,700$  neurons per  $\text{mm}^3$ ;  $n = 4$  mice per group;  $p < 0.05$ ) and 12-month-old transgenic mice (~47%;  $16,100 \pm 1,900$  vs.  $30,200 \pm 2,600$ ;  $n = 3$  mice per group) when compared to Control ( $p < 0.05$ ; Fig. 2b). While the dopaminergic neuron density remained on a similar level in transgenic  $\alpha$ -SYN mice of both ages ( $p > 0.05$ ), a clear trend towards an increase in these neurons was apparent in wild-type mice from 6 to 12 months ( $p = 0.06$ ), consistent with previous reports<sup>15</sup>. Collectively, these results demonstrate a sensitivity of dopaminergic PGNs to toxic A30P  $\alpha$ -SYN in the PD mouse model.

To confirm the negative effect of A30P  $\alpha$ -SYN deposition on the survival of newborn dopaminergic PGNs, we performed BrdU-injections (Fig. 2c–e). Of note, A30P  $\alpha$ -SYN mice showed ~50% reduction of the total new PGNs after 1 month ( $0.9 \pm 0.01\%$ ;  $n = 6$  mice vs.  $1.8 \pm 0.3\%$  in Control;  $n = 5$  mice;  $p < 0.05$ ) (Fig. 2d), whereas cell proliferation was not affected ( $p > 0.05$ ; not shown). Similar analysis in the GC layer revealed a comparable result: ~45% less adult-born GCs in the PD-like mice ( $2.0 \pm 0.1\%$ ;  $n = 6$  vs.  $3.6 \pm 0.5\%$  in Control;  $n = 5$ ) ( $p < 0.01$ ; not shown). The fraction of newborn dopaminergic PGNs, characterized by co-expressing of TH and BrdU, was decreased to ~33% in the PD-like mice ( $27.7 \pm 3.8\%$ ;  $n = 4$  mice/97 cells vs.  $41.6 \pm 3.4\%$ ;  $n = 3$  mice/91 cells, respectively;  $p < 0.05$ ) (Fig. 2e). As expected, the loss of dopaminergic adult-born PGNs was less than in PDGF $\beta$ -human A53T  $\alpha$ -SYN

mice<sup>12</sup> (70%), PDGF $\beta$ -human wild-type  $\alpha$ -SYN mice<sup>11</sup> (59%), and CaMK-human A30P  $\alpha$ -SYN mice<sup>13</sup> (41%). Together, these results confirm the reduced survival of adult-born PGNs and GCs in the OB of A30P  $\alpha$ -SYN mice, with the dopaminergic PGNs as one vulnerable subpopulation.

### Genetic labelling of dopaminergic neurons in A30P $\alpha$ -SYN mice.

To specifically target dopaminergic PGNs for the *in vivo* study in  $\alpha$ -SYN mice, we established a Cre/lox mouse model of PD (Fig. 3a). We first crossed knock-in driver lines expressing Cre recombinase from the TH locus (TH::IRES-Cre)<sup>42</sup> with tdTomato reporter mice<sup>43</sup>. These double-transgenic wild-type mice were referred to as TH-Control. Further crossing to Thy1-human A30P  $\alpha$ -SYN mice<sup>26</sup> enables the analysis of dopaminergic neurons with PD-like phenotype, cited as TH-A30P  $\alpha$ -SYN. Previous studies reported a non-specific leak in this Cre/lox system<sup>15,43</sup>. To test the accuracy of genetic labelling of dopaminergic neurons within the glomerular layer of TH-Control and TH-A30P  $\alpha$ -SYN mice (9-month-old), we stained OB sections with antibodies against TH and two other PGN markers<sup>39</sup>, Calbindin (CB) and Calretinin (CR) (Fig. 3b–d). In accordance with Adam and Mizrahi<sup>15</sup>, we detected tdTomato expression in the GC and MC layer (Fig. 3b), regions in which neurons normally do not express TH. Around the glomeruli, quantification of single and double-labelled neuronal somata expressing tdTomato with or without marker (Fig. 3c,d), revealed a majority of  $71.0 \pm 4.8\%$  tdTomato-positive cells expressing simultaneously TH ( $n = 3$  mice/1,698 cells). A very small proportion of tdTomato cells expressed CR ( $5.0 \pm 7.5\%$ ;  $n = 4$  mice/2,752 cells), while nearly none expressed CB ( $0.3 \pm 0.2\%$ ;  $n = 4$  mice/2,313 cells). To confirm stability of this labelling system within the time window for two-photon imaging, we compared these results to 12-month-old mice, revealing similar levels of tdTomato-positive cells expressing TH ( $69.9 \pm 2.6\%$ ;  $n = 2$  mice/226 cells;  $p > 0.05$ ). Overall, these findings are similar to previous reports<sup>15</sup> using heterozygous Z/EG GFP Cre reporter mice for the labelling of dopaminergic PGNs. Two months after transduction of new neurons with lentiviral (LV) eGFP constructs<sup>41,44</sup> in the rostral migratory stream (RMS), we observed a small fraction of cells being positive for both eGFP and tdTomato (Fig. 3e), confirming that the TH-A30P  $\alpha$ -SYN mouse labels adult-born dopaminergic PGNs. In conclusion, we consider this Cre/lox system appropriate for the genetic targeting of dopaminergic PGNs in the OB of transgenic  $\alpha$ -SYN mice.

### A30P $\alpha$ -SYN interferes with the stable integration of adult-born dopaminergic neurons *in vivo*.

To monitor the dynamic integration and fate of the adult-born PGNs *in vivo*, we implanted an open-skull cranial window over both OBs (Fig. 4a–d). In line with previous reports for the OB<sup>15</sup> and cortex<sup>45</sup>, we achieved with our preparation a success rate of ~60% usable windows for high-quality microscopy. Optical clarity for intravital two-photon imaging remained stable throughout the test period of 2.5 months. As open-skull surgery is associated with activation of glial cells in the OB<sup>15</sup> and cortex<sup>46</sup> within the first three weeks after operation, we started imaging 4 weeks post operatively to avoid the potential impact of gliosis on the analysis (Fig. 4e). Chronic imaging was performed in 9-month-old TH-A30P  $\alpha$ -SYN and aged-matched TH-Control mice. Assuming a continuous neuronal turnover, we chose this time frame to elucidate in more detail the lack of dopaminergic PGNs observed in 6- and 12-month-old transgenic  $\alpha$ -SYN mice (Fig. 2b). Because differentiation into the final fate of adult-born neurons requires synaptic contacts<sup>23,47</sup>, the appearance of tdTomato-labelled cell bodies indicated synaptic integration of newborn dopaminergic PGN, whereas disappearance of red somata clearly displayed the death of these neurons within the interneuron network<sup>15,48</sup> (Fig. 4f,g). Accordingly, all the stable, lost or gained PGNs were tracked in a 2-week interval as summarized in Fig. 4h. In both genotypes, the neuron turnover rates were similar ( $0.8 \pm 0.1$ ;  $n = 4$  mice/1,454 cells and  $0.6 \pm 0.2$ ;  $n = 5$  mice/1,437

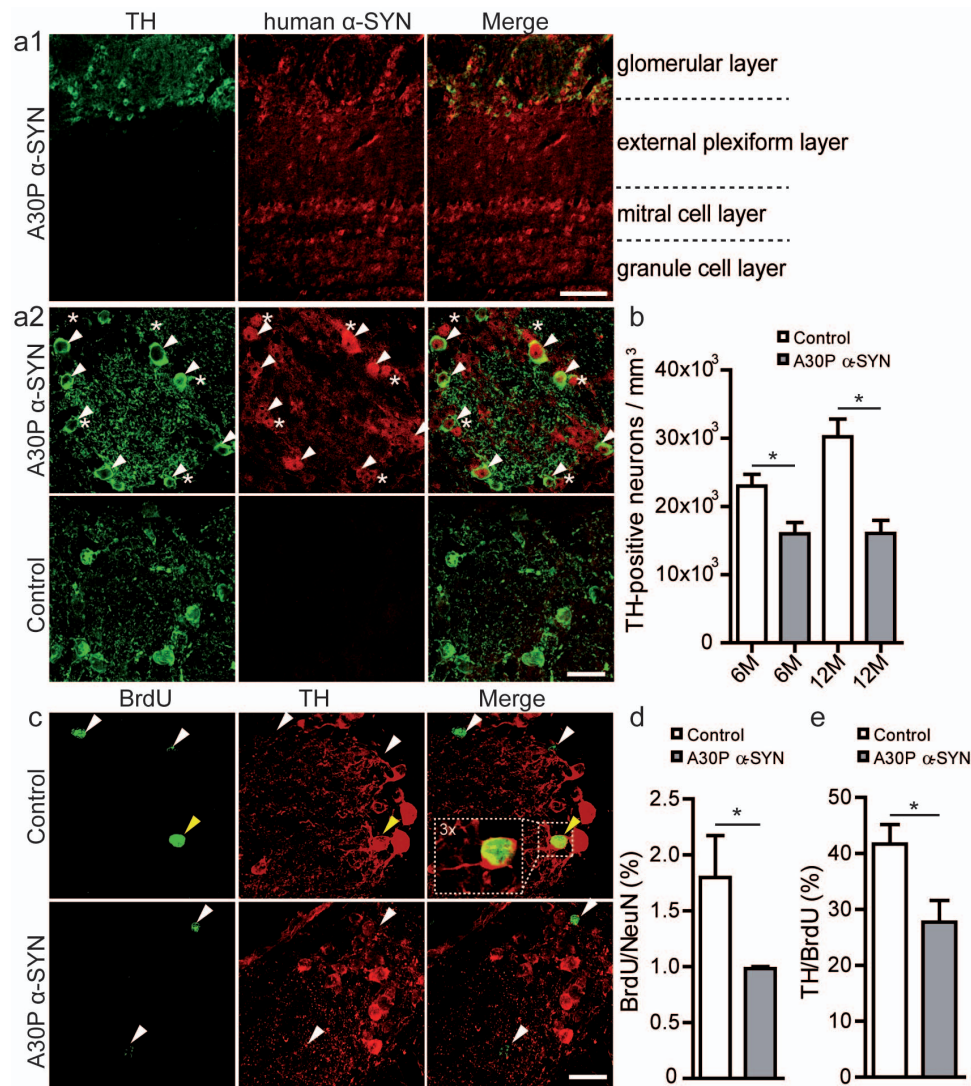


**Figure 2 | Reduced survival of adult-born periglomerular neurons in A30P  $\alpha$ -SYN mice.** (a1) Immunofluorescent micrographs demonstrating tyrosine hydroxylase (TH, green) and human A30P  $\alpha$ -SYN (15G7, red) expression in the various OB layers in transgenic  $\alpha$ -SYN mice: z-stack projections of confocal series. Scale bar - 50  $\mu$ m. Note that TH expression is restricted to the glomerular layer. (a2) Representative higher magnification images of one glomerulus shows accumulation of human A30P  $\alpha$ -SYN in dopaminergic neurons (white arrows) and other PGN subtypes (white asterisks) in A30P  $\alpha$ -SYN mice, whereas Control mice lack the expression of human  $\alpha$ -SYN. Scale bar - 20  $\mu$ m. (b) Summary plots showing the density of TH-positive neurons per mm<sup>3</sup> OB in 6- and 12-month-old Control ( $n = 8$ ) and A30P  $\alpha$ -SYN mice ( $n = 8$ ). (c) Representative immunofluorescent micrographs of adult-born (BrdU, green) dopaminergic (TH, red) neurons: z-stack projections of confocal series. Double-labelled cells (yellow arrow) represent a small fraction of the generally low number of BrdU-positive PGNs. Scale bar - 20  $\mu$ m. (d) Summary plots demonstrating the percentage of adult-born (BrdU) PGNs (NeuN) amongst all PGNs one month after their birth in 6-month-old Control ( $n = 4$ ) and A30P  $\alpha$ -SYN mice ( $n = 3$ ). (e) Summary plots showing the fraction of dopaminergic (TH) adult-born (BrdU) PGNs in Control ( $n = 4$ ) and A30P  $\alpha$ -SYN mice ( $n = 3$ ) of the same age. \* $p < 0.05$ ; Student's  $t$ -test.

cells; PD-like and Control, respectively) ( $p > 0.05$ ; not shown). Of note, in TH-Control mice more PGNs gradually added to the network as assessed relative to the first imaging time point (Fig. 4i), resulting in a steady increase of these neurons up to  $16.1 \pm 5.5\%$  after 2.5 months ( $p < 0.01$ ). This continuous enlargement of the dopaminergic PGN population in wild-type mice both confirms our results shown in Fig. 2b and accords with a previous study of dopaminergic neuron turnover<sup>15</sup>. In contrast, in TH-A30P  $\alpha$ -SYN mice the number of PGNs marginally decreased over time to  $-3.8 \pm 2.4\%$ , but statistically remained on the same level (Fig. 4i;  $p > 0.05$ ). Comparison of the fractional changes in the neuron density of both genotypes revealed significant differences at the last two time points ( $p < 0.05$  and  $p < 0.01$ , respectively). In addition, we determined the percentage of stable, lost and gained PGNs per imaging interval in both groups (Fig. 4k–m). Interestingly, both

genotypes showed similar fractions of gained PGNs (Fig. 4i;  $10.2 \pm 1.4\%$  vs.  $10.7 \pm 0.9\%$ ; PD-like and Control, respectively), while a significant increase in lost PGNs was recorded in the transgenic  $\alpha$ -SYN mice (Fig. 4m;  $11.4 \pm 1.1\%$  vs.  $7.6 \pm 1.0\%$ ;  $p < 0.05$ ). To determine the timing of cell loss, we further quantified the fraction of cells that appeared at one imaging time point, but quickly disappeared in the next, as a parameter for integration stability (Fig. 4n). This readout further provides novel insight into the temporal definition of the toxic effect of A30P  $\alpha$ -SYN. Notably, TH-A30P  $\alpha$ -SYN mice showed more than double the amount of 'short-lived' cells per imaging interval compared to TH-Control ( $28.2 \pm 1.2\%$  vs.  $12.7 \pm 3.9\%$ ;  $p < 0.05$ ). The higher neuron loss in PD-like mice was also reflected in a lower fraction of stable neurons ( $86.6 \pm 2.7\%$  vs.  $92.2 \pm 0.8\%$ ) ( $p = 0.06$ ; Fig. 4k) and a 23% decrease in the overall survival rate over time (Fig. 4j). Indeed,

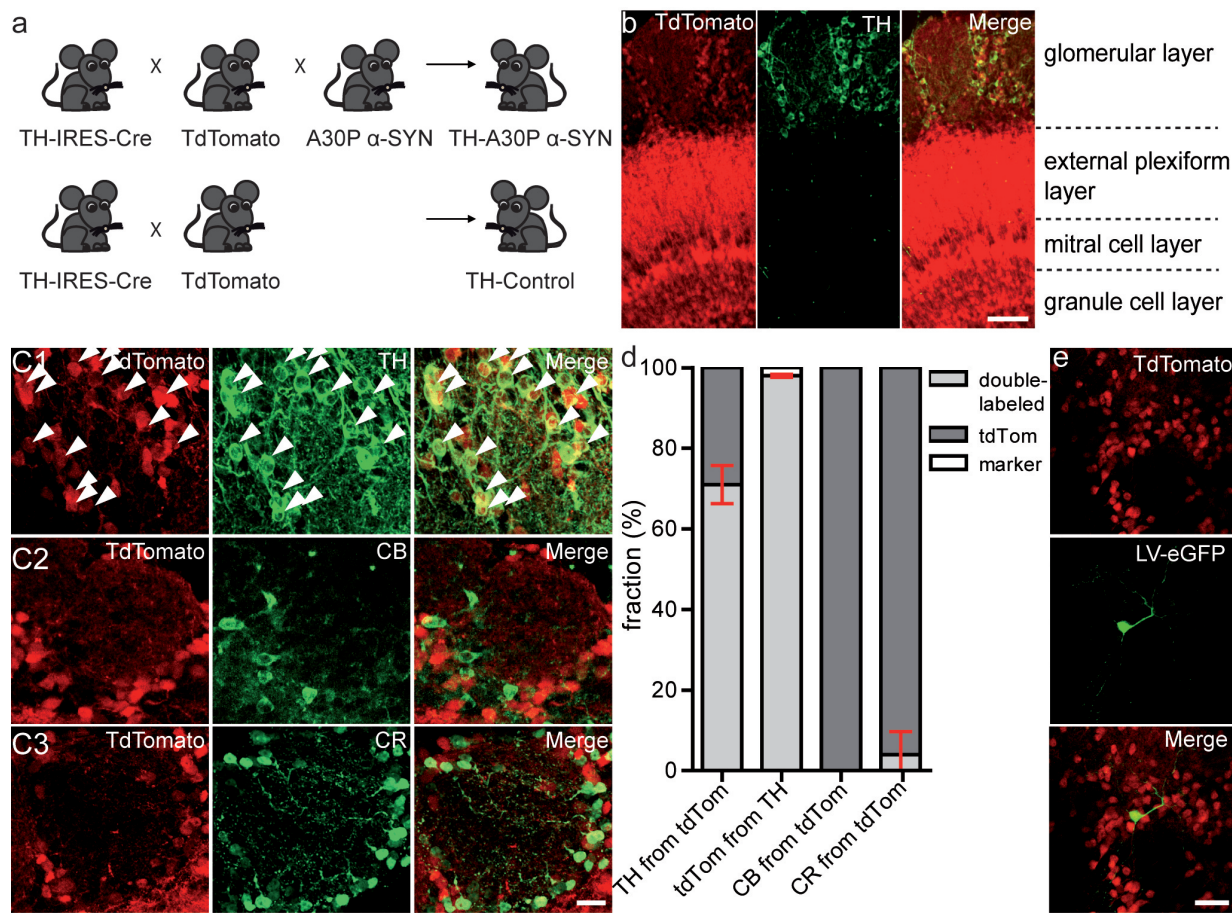


**Figure 3 | Genetic labelling of dopaminergic neurons in the olfactory bulb of A30P  $\alpha$ -SYN mice.** (a) Crossing scheme for targeting dopaminergic neurons in PD-like (top) and Control (wild-type; bottom) mice. Mice with Cre recombinase knocked into the TH locus were crossed to Ai9 tdTomato Cre reporter (TH-Control); and further to human A30P  $\alpha$ -SYN mice (TH-A30P  $\alpha$ -SYN). (b) Immunofluorescent micrographs showing tdTomato (red) and TH (green) expression in various OB layers in TH-A30P  $\alpha$ -SYN mice, including ‘Merge’ view: z-stack projections of confocal series. Scale bar - 50  $\mu$ m. (c) Representative high magnification images of one glomerulus with tdTomato-positive PGNs, stained for various subtype markers (c1) TH, (c2) calbindin (CB) or (c3) calretinin (CR) (green): z-stack projections of confocal series. White arrows point to double-labelled cells (Merge, yellow). Scale bar - 20  $\mu$ m. (d) Summary plots showing the percentage of single/double-labelled PGN somata in TH-A30P  $\alpha$ -SYN mice, expressing tdTomato with or without TH, CR and CB. TH from tdTomato, 71.0  $\pm$  4.8% of tdTomato-positive cells expressed TH; tdTomato from TH, 98.0  $\pm$  0.4% of TH cells expressed tdTomato ( $n$  = 1,698 cells from 3 mice); CB from tdTomato, 0.3  $\pm$  0.2% of tdTomato-positive cells expressed CB ( $n$  = 2,313 cells from 4 mice); CR from tdTomato, 5.0  $\pm$  7.5% of tdTomato-positive cells expressed CR ( $n$  = 2,752 cells from 4 mice). (e) High-resolution micrograph of a 2-month-old lentivirally-labelled (LV-eGFP; green) dopaminergic (tdTomato; red) adult-born PGN in TH-A30P  $\alpha$ -SYN mice: z-stack projections of *in vivo* two-photon series. Scale bar - 20  $\mu$ m.

while 70.9  $\pm$  5.5% PGNs, counted in TH-Control at the first time point, were still preserved after 2.5 months, this number was reduced to 54.7  $\pm$  8.3% in TH-A30P  $\alpha$ -SYN mice ( $p$  < 0.05). In conclusion, this detailed turnover analysis reveals deleterious consequences of A30P  $\alpha$ -SYN on the stable incorporation of new PGNs, which reach the glomerular layer and appear to integrate into the abnormal ‘diseased’ network but are eliminated shortly afterwards.

## Discussion

Our study provides the first *in vivo* evidence that A30P  $\alpha$ -SYN accumulation interferes with the stable integration of the adult-born neurons in the OB, with significant effects on their survival. As summarized in Fig. 5, we describe a progressive increase in cell loss in the transgenic mutant  $\alpha$ -SYN mice (~12%) as compared to wild-type (~8%), while at the same time the gain in new neurons is similar in both groups (~10%). Of note, this neuronal loss specifically targets those cells which have been recently integrated in the network. Such data demonstrates that early stages of incorporation and differentiation into dopaminergic neurons are not affected in transgenic Thy1-A30P  $\alpha$ -SYN mice. Rather, it is their longer-term consistency

and survival within the OB network which is defective, resulting in an overall reduction in the net addition of neurons to the OB over time. Consequently, PD-like mice lack the successful substitution of pre-existing adult-born neurons with new functional cells. Maintaining a stable, and precise, equilibrium between the influx of new neurons and the elimination of old neurons represents a key determinant of olfactory discrimination<sup>49</sup>. We therefore propose a disturbed neuronal plasticity resulting from unstable integration of adult-born PGNs and GCs in A30P  $\alpha$ -SYN mice, as a probable contributing factor to the observed olfactory discrimination deficits.

Furthermore, with this chronic, intravital two-photon imaging study of the integration kinetics of new neurons in transgenic  $\alpha$ -SYN mice, we have also developed a potentially useful platform for the testing and evaluation of drugs that promote the integration and survival of neurons against  $\alpha$ -SYN-induced toxicity. For this purpose, the OB is ideal since it is located superficially and thus easy to access<sup>15</sup>, whilst representing at the same time the second main source of dopaminergic neurons in the brain<sup>50</sup>. We studied this subset of adult-born neurons as representative of a vulnerable population of interneurons. Their susceptibility to increased amounts of  $\alpha$ -SYN

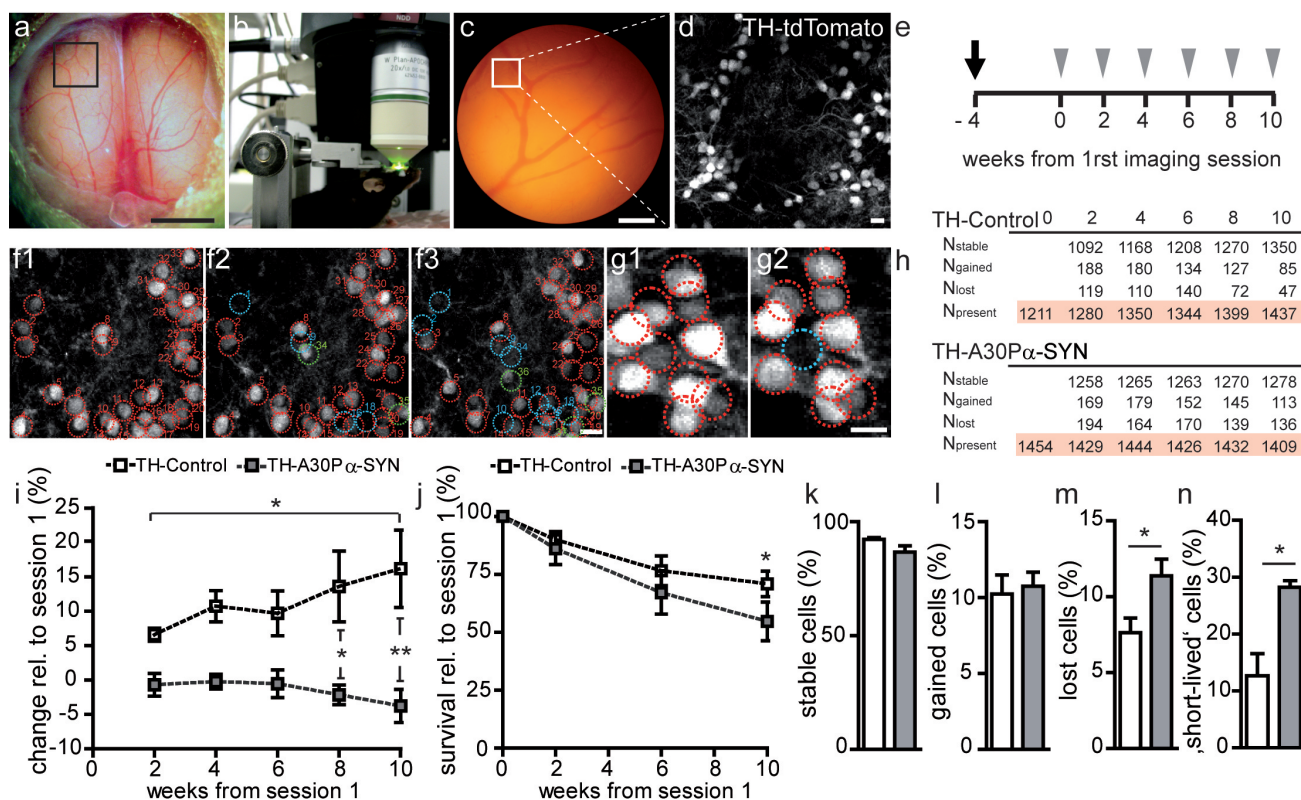


**Figure 4 | Unstable integration of dopaminergic neurons in TH-A30P  $\alpha$ -SYN mice *in vivo*.** (a, b) Intravital two-photon microscopy of dopaminergic neuron turnover through a 3 mm round open-skull cranial window implanted over both OBs. Scale bar - 1 mm (a). (c) Blood vessel map of the region of interest (black box), as defined in (a). Scale bar - 100  $\mu$ m. (d) Representative micrograph of the position (white box) marked in (c) with tdTomato-labeled dopaminergic PGNs: z-stack projection of two-photon image series. Scale bar - 10  $\mu$ m. (e) Experimental time scheme of window surgery (black arrow) followed by *in vivo* two-photon imaging (grey arrow heads) in a two-week interval for a period of 2.5 months. Mice were 8 month old at the time point of surgery. Tracking of stable (red), gained (green) and lost (blue) PGNs in the (f1) first, (f2) second, and (f3) third imaging session, respectively: z-stack projection of two-photon image series. Scale bar - 10  $\mu$ m. (g1, g2) High-magnification images of tdTomato-labelled PGNs: (g2) one lost cell (blue) in between a majority of stable somata (red) in two consecutive imaging sessions. Scale bar - 10  $\mu$ m. (h) Table with absolute cell counts for stable ( $N_{\text{stable}}$ ), lost ( $N_{\text{lost}}$ ), gained ( $N_{\text{gained}}$ ) and present ( $N_{\text{present}}$ ) cells at various imaging time points in both genotypes. (i) Quantification of the change (in %) in the PGN population over time relative to the first imaging session in TH-Control ( $n = 5$ ) and TH-A30P  $\alpha$ -SYN mice ( $n = 4$ ). (j) Quantification of the neuronal survival rate (in %) relative to the first imaging session in TH-Control ( $n = 5$ ) and TH-A30P  $\alpha$ -SYN mice ( $n = 4$ ). Summary plots showing the fraction of (k) stable, (l) gained, (m) lost, and (n) 'short-lived' neurons per imaging interval (%) in TH-Control ( $n = 5$ ) and TH- $\alpha$ -SYN mice ( $n = 4$ ). Note the high fraction of 'short-lived' neurons in TH-A30P  $\alpha$ -SYN mice, namely PGNs which appeared in one session but quickly disappeared in the following. \* $p < 0.05$ , \*\* $p < 0.01$ ; one way ANOVA/Tukey-Kramer post-hoc test (i); two-way ANOVA/Bonferroni post-hoc test (i,j); Student's *t*-test (k-n).

had been demonstrated by several other studies, analysing variously proliferation, differentiation, survival and signalling of dopaminergic PGNs<sup>11–14,28</sup>. A possible explanation for the vulnerability of dopaminergic neurons involves increased cellular toxicity in the presence of dopamine<sup>51</sup>. Other groups report on the role of  $\alpha$ -SYN in regulating dopamine biosynthesis, which is disturbed upon  $\alpha$ -SYN aggregation<sup>52</sup>. We further showed that increased cell death is not a unique feature of dopaminergic adult-born PGNs but appears also in other integrating neurons, because adult-born GCs were affected similarly in our PD mouse model as well as in others<sup>11–14</sup>.

The observed effects on the sensitive, newly-integrating neurons could originate from different sources, namely (i) intracellular  $\alpha$ -SYN toxicity, or (ii) extrinsic influence from the  $\alpha$ -SYN loaded network/ $\alpha$ -SYN pathology in MCs. The latter possibility implicates that  $\alpha$ -SYN accumulation in the OB network is likely to alter the synaptic activity of the neuronal circuit. During maturation and integration, roughly between 10 and 60 days after birth, adult-born neurons establish synapses with existent neurons<sup>21,23</sup>. Thereafter, cells may remain stable for up to 19 months, indicating long-term survival of the adult-born cells<sup>47</sup>. Our study specifically reveals that the critical step between early and stable integration/survival of the adult-born

neurons, which depends on neuronal input and activity<sup>16</sup>, is affected by A30P  $\alpha$ -SYN aggregation. In favour of the altered network hypothesis, we show that transgenic A30P  $\alpha$ -SYN mice are characterized by broad  $\alpha$ -SYN accumulation in the OB, while only MCs - the main synaptic partners of adult-born PGNs and GCs<sup>25</sup> - have pathology-associated  $\alpha$ -SYN modifications<sup>36</sup>. Interestingly, Thy1 expression in the OB starts in MCs<sup>53</sup>, and transgene expression under Thy1 increases with neuron maturation<sup>32,53</sup>. We thus attribute the specific location of the  $\alpha$ -SYN pathology in MCs to their stability within the OB network, allowing gradual accumulation and deposition of the protein, whereas dynamic populations of PGNs and GCs are constantly replaced during adult neurogenesis. Indeed, this  $\alpha$ -SYN phosphorylation in MCs could present also a protective mechanism against the increasing amount of more soluble protein species (e.g. monomers, oligomers) as postulated recently by Oueslati *et al.*<sup>54</sup>. Notably, both dopaminergic PGNs (and GCs) lack the aggregated/phosphorylated form of  $\alpha$ -SYN, but still get lost. From maturation on, these cells contain high amounts of human  $\alpha$ -SYN with a point mutation which is known to accelerate the association into toxic oligomers<sup>29,30</sup>. These mediate intracellular  $\alpha$ -SYN toxicity - a widely accepted disease mechanism<sup>27</sup> - especially during the critical phase of

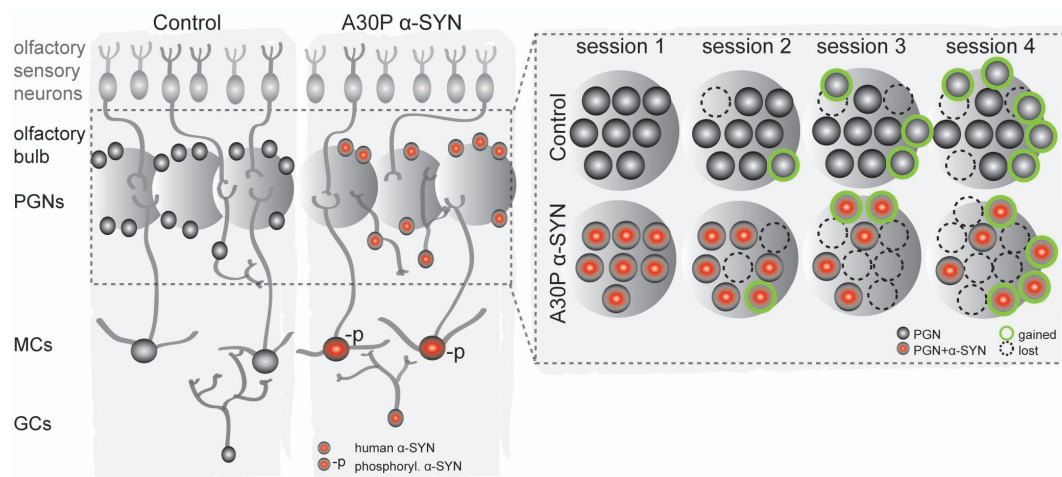


**Figure 5 | Integration model for adult-born neurons in A30P  $\alpha$ -SYN mice.** (left - overview) Adult-born PGNs and GCs integrate into the pre-existing OB network to contribute to olfactory function. In PD-like mice, new neurons face an  $\alpha$ -SYN-loaded network (red; enhanced A30P  $\alpha$ -SYN expression) with a pathology-associated phenotype in MCs (-p; phosphorylated  $\alpha$ -SYN), the central synaptic partners of both PGNs and GCs. (right - crop into the glomerular layer) Our *in vivo* study of dopaminergic PGN turnover provides evidence for a shortened survival of adult-born neurons due to unstable integration. While same fractions of cells are gained in both groups ( $\sim 10\%$ ; green border), transgenic  $\alpha$ -SYN mice show a higher cell loss ( $\sim 12\%$ ) than wild-type ( $\sim 8\%$ ; broken border). Of note, this neuronal loss specifically targets those cells which have been recently integrated in the network, the 'short-lived' neurons. This imbalance results in a reduction in the addition of neurons to the glomerular layer over time in PD-like mice. These data suggest that increased  $\alpha$ -SYN accumulation - both inside the affected cell and in the surrounding network - drastically interferes with the balanced turnover of old and new neurons by preventing stable, longer-term integration of new neurons. An impaired homeostasis of functional new neurons represents a likely contributor to odour discrimination deficits in A30P  $\alpha$ -SYN mice.

synaptic integration<sup>16,17</sup>. Moreover, extracellular effects on the new neurons by secreted protein<sup>54</sup> are possible. Definitely, the total dosage of  $\alpha$ -SYN is a significant factor to determine its toxicity in the cause of PD<sup>55,56</sup>.

In conclusion, we demonstrate the pathological effects of aggregation-prone A30P  $\alpha$ -SYN on the homeostatic turnover of adult-born neurons, and on their stability and longer-term survival during integration into the OB network. Therefore, our transgenic mouse model with late Thy1-A30P  $\alpha$ -SYN expression reflects, in part, the pathology observed in brains of PD patients with Lewy bodies in MCs of the OB<sup>7,8</sup>, the human olfactory deficit at an early stage of the disease process<sup>1-3</sup> and a lack of progenitor cells<sup>10</sup>. Importantly, our results support the previously reported association between adult neurogenesis and fine odour discrimination<sup>49,57,58</sup>, although we still lack the molecular and cellular mechanism to explain olfactory deficits in these mice<sup>59</sup>. Finally, a detailed investigation of the dendritic and synaptic maturation of these neurons along with an analysis of their synaptic connectivity to MCs will better our understanding of the effects of toxic/mutant/aggregated  $\alpha$ -SYN on odour discrimination deficiency in transgenic  $\alpha$ -SYN mice.

## Methods

**Animals.** We used adult mice (5–12-month-old) that were bred and maintained in a specified pathogen-free animal facility: transgenic mice (C57Bl6 background) overexpressing human A30P  $\alpha$ -SYN under control of the Thy1-promoter<sup>26</sup> and age-matched wild-type mice with same genetic background. For specific labeling of dopaminergic PGNs in A30P  $\alpha$ -SYN (1) and wild-type mice (2), the following two lines were crossed: (1) TH::IRES-Cre driver line<sup>42</sup>xAi9 tdTomato Cre reporter line with floxed stop codon<sup>43</sup>xA30P  $\alpha$ -SYN line<sup>26</sup>, cited as TH-A30P  $\alpha$ -SYN; (2) TH::IRES-Cre driver line<sup>42</sup>xAi9 tdTomato Cre reporter line<sup>43</sup>, referred to as TH-Control. In both lines, the floxed stop sequence is excised by the Cre enzyme and tdTomato expression is activated only in TH-positive neurons of the F1 offspring. All mice were kept in normal 12 h-light-dark cycle, had free access to food and water and showed no signs of inflammation or metabolic compromise. Genotypes were determined from mouse-tail DNA samples by PCR for tdTomato (forward primer: CTGTTCTGTACGGCATGG; reverse primer: GGCATT AAAGCAGCGTATCC) and human A30P  $\alpha$ -SYN (forward primer: ATGGATGTATTCATGAAAGG; reverse primer: TTAGGCTTCAGGTTTCGTAG). Together,  $n = 58$  animals were used in this study. All procedures were in accordance with an animal protocol approved by the University of Munich and the government of Upper Bavaria (Az. 55.2-1-54-2531-184-09).

**Immunohistochemistry and confocal microscopy.** Mice were perfused transcardially with 4% paraformaldehyde. For immunohistochemistry, the following primary antibodies were applied to 50  $\mu$ m free-floating coronal OB sections: mouse monoclonal anti-tyrosine hydroxylase (TH) (1 : 500), anti-calretinin (CR) (1 : 1000) and anti-NeuN (1 : 200) from Millipore, mouse monoclonal anti-calbindin (CB) (1 : 500) from Sigma, rat monoclonal anti-BrdU (1 : 200), rabbit monoclonal pSer129  $\alpha$ -SYN (1 : 500) from Abcam, and rat monoclonal antibody 15G7 against human  $\alpha$ -SYN (116–131) peptide MPVDPDNEAYEMPSEE (1 : 4000) from Connex<sup>31</sup>. As secondary antibodies, we used: goat anti-mouse Alexa 488/647 (1 : 500), rabbit anti-rat Alexa 488/647 (1 : 500) from Invitrogen and biotinylated rabbit anti-rat (1 : 300) from Dako. Enzymatic digestion using Proteinase K (PK; Roche) was employed for 8–10 min. Peroxidase detection was applied for 8–10 min (DAB detection kit, DCS Diagnostics). Sections were imaged at 0.75  $\mu$ m pixels resolution in xy dimension and 1  $\mu$ m in z dimension on a confocal microscope (Zeiss LSM 510) equipped with a 10 $\times$ , 25 $\times$  or 40 $\times$  oil objective (Zeiss). Counting of somata and nuclei was performed manually from confocal image stacks, using Zeiss AIM software. For consistent analysis, every tenth OB slice was used and imaged at predefined positions within the glomerular layer.

**BrdU injections.** To study of the survival of adult-born neurons, 5-month-old mice received intraperitoneal (i.p.) injections of bromodeoxyuridine (BrdU; 50 mg/kg) for 5 consecutive days, and were perfused transcardially at 32 days after the 1st injection<sup>11</sup>. To test possible effects of A30P  $\alpha$ -SYN on the proliferation of new cells, the mice received one single BrdU injection (100 mg/kg; i.p.), and were perfused after 24 hrs.

**Viral injection and open-skull craniotomy.** Mice were deeply anaesthetized with ketamine/xylazine (0.13/0.01 mg/g body weight; i.p.). Additionally, dexamethasone (6  $\mu$ g/g body weight; i.p.; Sigma) was administered before surgery. Stereotaxic injection of LV particles for the transduction of adult-born neurons was performed, using pressure via a micropipette<sup>44</sup>. Mouse received 300 nl injection on both left and right RMS (coordinates relative to Bregma: anterior -3.3 mm, lateral -0.8 mm, depth 2.9 mm), where new dopaminergic neurons are predominantly generated<sup>40,41</sup>. Lentivirus, containing the gene for eGFP, controlled by the CAG promoter (plasmids from Dr. Stylianos Michalakis) was used at a titer of  $>10^8$  infecting units ml<sup>-1</sup>. Implantation of open-skull cranial windows over both OBs was performed in eight-month-old mice as described elsewhere<sup>15</sup>. Briefly, the skull over both OBs was cleaned and dried. A round 3 mm craniotomy was opened over both OB hemispheres. Bone was carefully removed and a 3 mm round cover slip (VWR) was gently placed on the cavity and glued to the bone with thin layers of Histoacryl glue (B. Braun) and dental cement (Cyano Veneer fast; H. Schein). For repeated imaging in a custom-made stereotaxic stage, a 0.1 g metal bar was glued to the skull. After surgery, mice received a subcutaneous analgesic dose of carprofen (5  $\mu$ g/g body weight Rimadyl; Pfizer) and the antibiotic cefotaxime (0.25 mg/g body weight, Pharmore) for three days. Imaging began after a resting period of four weeks. In  $\sim 60\%$  of the animals (9/15 mice) the brain region under the window was clear for imaging. If new bone grew



under the window and impeded high-quality imaging, mice were excluded from the study.

**In vivo two-photon imaging.** Imaging was performed under light anaesthesia (ketamine/xylazine, 0.1/0.0075 mg/g body weight, i.p.). Mice were placed under the microscope in a custom-made holder with fixed position relative to the objective lens. Two-photon imaging data presented here were from 6 consecutive imaging sessions from 9 mice. First imaging took place four weeks after surgery (time point 0), then imaging continued up to 2.5 months in a two-week interval. Imaging was performed using an upright two-photon microscope (Zeiss), equipped with a 20× water immersion objective (1.0 NA; Zeiss). TdTomato was excited with a femtosecond laser (MaiTai DeepSee, Spectra-Physics) at 915 nm and emission was collected at 527–582 nm, respectively (LSM 7MP, Zeiss). Images of cell bodies were acquired at 0.41 μm pixels resolution in xy dimension and 2 μm in z dimension (1024 × 1024 pixels). Same imaging volumes were precisely aligned over the imaging period. The laser intensity was adjusted to keep the emitted tdTomato fluorescence stable.

**Olfaction tests.** To detect differences in olfactory performance, 6-month-old mice were tested in a smell discrimination task<sup>37,38</sup>. Briefly, before the start of the experiment, mice were placed on a restricted diet to maintain a 10% reduced body weight during training and testing phase. Odorants were presented on fresh shavings (1 ml per 3 g shavings) in 2 round plastic dishes, mounted horizontally on a carrier, and separated by a vertical barrier between them. During training, the mice learned to dig in a dish with unscented shavings to find a small piece of chocolate. For the discrimination tasks, two identical dishes were presented simultaneously on the carrier. In the beginning, one dish was scented with apple odorant (designated as S<sup>+</sup>; 10% Phenethylacetate; Sigma) and the other with the same amount of solvent (Diethylphthalate; Sigma). Digging in the S<sup>+</sup> dish was consistently rewarded with chocolate. To train the mice to associate the smell of S<sup>+</sup> (and not of chocolate) with the reward, the chocolate was now buried in both scented shavings (15 successful trials). Mice had to discriminate between S<sup>+</sup> and strawberry odorant (S<sup>-</sup>; 10% Methyl trans-cinnamate; Sigma). To increase the level of difficulty, the mice had to discriminate between different binary mixtures of S<sup>+</sup> and S<sup>-</sup> with increasing similarity between the odours, [S<sup>+</sup>:S<sup>-</sup>] vs. [S<sup>+</sup>:S<sup>-</sup>]: [70:30] vs. [30:70]; [55:45] vs. [45:55]; [53:47] vs. [47:53]; [51:49] vs. [49:51] and [50:50] vs. [50:50]. A correct choice was defined as digging in the dish with the higher amount of S<sup>+</sup> (8 trials/day). Successful choices were rewarded with a small piece of chocolate, whereas failed discrimination (choice of S<sup>-</sup>) immediately terminated the trial. To assess differences in olfactory long-term memory, the mice were confronted with the same odours again after 2 months, and the success in choosing the S<sup>+</sup> odour was evaluated (12 trials).

**Data analysis and statistics.** Quantitative analysis of neuron turnover was performed manually from two-photon image stacks, using Zeiss AIM software. From each stack in consecutive imaging sessions, several regions of interest were identified and cropped. Stacks were z-projected and each region of interest was compared with the same region in the previous session. Thereby, each cell was manually scored as stable (N<sub>stable</sub>), lost (N<sub>lost</sub>), or new (N<sub>gained</sub>). Turnover ratios representing the gain and loss of neurons from day to day were calculated as dTOR = (N<sub>gained</sub> + N<sub>lost</sub>)/(2 × N<sub>present</sub>)/I<sub>t</sub>, where N<sub>present</sub> is the number of all apparent neurons at a time point and I<sub>t</sub> is the number of days between subsequent imaging sessions<sup>60</sup>. Fractional changes in the neuron population were quantified for every time point relative to the first imaging session. Mean fractions of stable, lost and gained neurons were calculated for each time point and mouse. In addition, the fractions of cells which were gained at one time-point, but immediately lost in the following, were quantified as parameter for neuronal integration stability. Neuronal survival rates were measured at 2, 6 and 10 weeks relative to session 1. For statistical comparison of the two test groups over various time points, we applied two-way ANOVA with Bonferroni post-hoc test. To compare changes inside one group, we used one-way ANOVA with repeated measures, followed by Tukey-Kramer post-hoc test. To evaluate the success rates of both groups at various odour mixtures, we applied two-way ANOVA with Bonferroni post-hoc test. Unpaired Student's *t*-test was used to assess neuron numbers and olfactory memory. Significance was accepted at *p* < 0.05. Data were illustrated as mean ± SEM or mean ± SD.

- Doty, R. L., Riklan, M., Deems, D. A., Reynolds, C. & Stellar, S. The olfactory and cognitive deficits of Parkinson's disease: evidence for independence. *Ann. Neurol.* **25**, 166–177 (1989).
- Parrao, T. *et al.* Olfactory deficits and cognitive dysfunction in Parkinson's disease. *Neurodegener. Dis.* **10**, 179–182 (2012).
- Berendse, H. W. *et al.* Subclinical dopaminergic dysfunction in asymptomatic Parkinson's disease patients' relatives with a decreased sense of smell. *Ann. Neurol.* **50**, 34–41 (2001).
- Haehner, A., Hummel, T. & Reichmann, H. Olfactory loss in Parkinson's disease. *Parkinsons Dis.* **2011**, 1–6 (2011).
- Spillantini, M. G. *et al.* Alpha synuclein in Lewy bodies. *Nature* **388**, 839–840 (1997).
- Daniel, S. E. & Hawkes, C. H. Preliminary diagnosis of Parkinson's disease by olfactory bulb pathology. *Lancet* **340**, 186 (1992).
- Ubeda-Bañon, I. *et al.* alpha-Synucleinopathy in the human olfactory system in Parkinson's disease: involvement of calcium-binding protein- and substance P-positive cells. *Acta Neuropathol.* **119**, 723–735 (2010).
- Braak, H. *et al.* Staging of brain pathology related to sporadic Parkinson's disease. *Neurobiol. Aging* **24**, 197–211 (2003).
- Fleming, S. M. *et al.* Olfactory deficits in mice overexpressing human wildtype alpha-synuclein. *Eur. J. Neurosci.* **28**, 247–256 (2008).
- Höglinger, G. U. *et al.* Dopamine depletion impairs precursor cell proliferation in Parkinson disease. *Nat. Neurosci.* **7**, 726–735 (2004).
- Winner, B. *et al.* Human wild-type alpha-synuclein impairs neurogenesis. *J. Neuropathol. Exp. Neurol.* **63**, 1155–1166 (2004).
- Winner, B. *et al.* Mutant alpha-synuclein exacerbates age-related decrease of neurogenesis. *Neurobiol. Aging* **29**, 913–925 (2008).
- Marxreiter, F. *et al.* Changes in adult olfactory bulb neurogenesis in mice expressing the A30P mutant form of alpha-synuclein. *Eur. J. Neurosci.* **29**, 879–890 (2009).
- May, V. E. L. *et al.* Impaired olfactory bulb neurogenesis depends on the presence of human wild-type alpha-synuclein. *Neuroscience* **222**, 343–355 (2012).
- Adam, Y. & Mizrahi, A. Long-term imaging reveals dynamic changes in the neuronal composition of the glomerular layer. *J. Neurosci.* **31**, 7967–7973 (2011).
- Ming, G. L. & Song, H. Adult neurogenesis in the mammalian brain: significant answers and significant questions. *Neuron* **70**, 687–702 (2011).
- Kelsch, W., Lin, C. W., Mosley, C. P. & Lois, C. A critical period for activity-dependent synaptic development during olfactory bulb adult neurogenesis. *J. Neurosci.* **29**, 11852–11858 (2009).
- Lledo, P. M., Alonso, M. & Grubb, M. S. Adult neurogenesis and functional plasticity in neuronal circuits. *Nat. Rev. Neurosci.* **7**, 179–193 (2006).
- Petreanu, L. & Alvarez-Buylla, A. Maturation and death of adult-born olfactory bulb granule neurons: Role of olfaction. *J. Neurosci.* **22**, 6106–6113 (2002).
- Rochefort, C., Gheusi, G., Vincent, J. D. & Lledo, P. M. Enriched odour exposure increases the number of newborn neurons in the adult olfactory bulb and improves odour memory. *J. Neurosci.* **22**, 2679–2689 (2002).
- Carlen, M. *et al.* Functional Integration of Adult-Born Neurons. *Current Biology* **12**, 606–608 (2002).
- Lazarini, F. & Lledo, P. M. Is adult neurogenesis essential for olfaction? *Trends Neurosci.* **34**, 20–30 (2011).
- Carleton, A., Petreanu, L. T., Lansford, R., Alvarez-Buylla, A. & Lledo, P. M. Becoming a new neuron in the adult olfactory bulb. *Nat. Neurosci.* **6**, 507–518 (2003).
- Shepherd, G. M., Chen, W. R., Willhite, D., Migliore, M. & Greer, C. A. The olfactory granule cell: from classical enigma to central role in olfactory processing. *Brain Res. Rev.* **55**, 373–382 (2007).
- Lepousez, G., Valley, M. T. & Lledo, P. M. The impact of adult neurogenesis on olfactory bulb circuits and computations. *Annu. Rev. Physiol.* **75**, 339–363 (2013).
- Kahle, P. J. *et al.* Subcellular localization of wild-type and Parkinson's disease-associated mutant alpha synuclein in human and transgenic mouse brain. *J. Neurosci.* **20**, 6365–6373 (2000).
- Cookson, M. R. & van der Brug, M. Cell systems and the toxic mechanism(s) of alpha-synuclein. *Exp. Neurol.* **209**, 5–11 (2008).
- Nuber, S. *et al.* Olfactory neuron-specific expression of A30P alpha-synuclein exacerbates dopamine deficiency and hyperactivity in a novel conditional model of early Parkinson's disease stages. *Neurobiol. Dis.* **44**, 192–204 (2011).
- Krüger, R. *et al.* Ala30Pro mutation in the gene encoding alpha-synuclein in Parkinson's disease. *Nat. Genet.* **18**, 106–108 (1998).
- Conway, K. A. *et al.* Acceleration of oligomerization, not fibrillization, is a shared property of both alpha-synuclein mutations linked to early-onset Parkinson's disease: implications for pathogenesis and therapy. *Proc. Natl. Acad. Sci.* **97**, 571–576 (2000).
- Neumann, M. *et al.* Misfolded proteinase K-resistant hyperphosphorylated alpha-synuclein in aged transgenic mice with locomotor deterioration and in human alpha-synucleinopathies. *J. Clinical Investigation* **110**, 1429–1439 (2002).
- Kollias, G., Spanopoulou, E., Grosveld, F., Ritter, M., Beech, J. & Morris, R. Differential regulation of a Thy-1 gene in transgenic mice. *Proc. Natl. Acad. Sci. USA* **84**, 1492–1496 (1987).
- Winner, B., Kohl, Z. & Gage, F. H. Neurodegenerative disease and adult neurogenesis. *Eur. J. Neurosci.* **33**, 1139–1151 (2011).
- Sato, H., Kato, T. & Arawaka, S. The role of Ser129 phosphorylation of alpha-synuclein in neurodegeneration of Parkinson's disease: a review of in vivo models. *Rev. Neurosci.* **9**, 1–9 (2013).
- Saito, Y. *et al.* Accumulation of phosphorylated alpha-synuclein in aging human brain. *J. Neuropathol. Exp. Neurol.* **62**, 644–654 (2003).
- Schell, H., Hasegawa, T., Neumann, M. & Kahle, P. Nuclear and neuritic distribution of Serine 129 phosphorylated alpha-SYN in transgenic mice. *Neuroscience* **160**, 796–804 (2009).
- Mihalick, S. M., Langlois, J. C., Krienke, J. D. & Dube, W. V. An olfactory discrimination procedure for mice. *J. Exp. Anal. Behav.* **73**, 305–318 (2000).
- Glasl, L. *et al.* Pink1-deficiency in mice impairs gait, olfaction and serotonergic innervation of the olfactory bulb. *Exp. Neurol.* **235**, 214–227 (2012).
- Kosaka, K. & Kosaka, T. Chemical properties of type 1 and type 2 periglomerular cells in the mouse olfactory bulb are different from those in the rat olfactory bulb. *Brain Res.* **1167**, 42–55 (2007).
- Ninkovic, J., Mori, T. & Götz, M. Distinct Modes of Neuron Addition in Adult Mouse Neurogenesis. *J. Neurosci.* **27**, 10906–10911 (2007).
- Hack, M. A. *et al.* Neuronal fate determinants of adult olfactory bulb neurogenesis. *Nature Neuroscience* **8**, 865–872 (2005).



42. Lindeberg, J. *et al.* Transgenic expression of Cre recombinase from the tyrosine hydroxylase locus. *Genesis* **40**, 67–73 (2004).
43. Madisen, L. *et al.* A robust and high-throughput Cre reporting and characterization system for the whole mouse brain. *Nat. Neurosci.* **13**, 133–140 (2010).
44. Livneh, Y. & Mizrahi, A. Experience-dependent plasticity of mature adult-born neurons. *Nat. Neurosci.* **15**, 26–28 (2011).
45. Holtmaat, A. *et al.* Long-term, high-resolution imaging in the mouse neocortex through a chronic cranial window. *Nat. Protoc.* **4**, 1128–1144 (2009).
46. Lee, W. C. *et al.* A dynamic zone defines interneuron remodeling in the adult neocortex. *Proc. Natl. Acad. Sci.* **105**, 19968–19973 (2008).
47. Winner, B., Cooper-Kuhn, C. M., Aigner, R., Winkler, J. & Kuhn, H. G. Long-term survival and cell death of newly generated neurons in the adult rat olfactory bulb. *Eur. J. Neurosci.* **16**, 1681–1689 (2002).
48. Sawada, M. *et al.* Sensory input regulates spatial and subtype-specific patterns of neuronal turnover in the adult olfactory bulb. *J. Neurosci.* **31**, 11587–11596 (2011).
49. Mouret, A., Lepousez, G., Gras, J., Gabellec, M. M. & Lledo, P. M. Turnover of newborn olfactory bulb neurons optimizes olfaction. *J. Neurosci.* **29**, 12302–12314 (2009).
50. Baker, H., Kawano, T., Margolis, F. L. & Joh, T. H. Transneuronal regulation of tyrosine hydroxylase expression in olfactory bulb of mouse and rat. *J. Neurosci.* **3**, 69–78 (1983).
51. Conway, K. A., Rochet, J. C., Bieganski, R. M. & Lansbury, P. T. Jr. Kinetic stabilization of the alpha-synuclein protofibril by a dopamine-alpha-synuclein adduct. *Science* **294**, 1346–1349 (2001).
52. Alerte, T. N. *et al.* Alpha-synuclein aggregation alters tyrosine hydroxylase phosphorylation and immunoreactivity: lessons from viral transduction of knockout mice. *Neurosci. Lett.* **435**, 24–29 (2008).
53. Xue, G. P., Calvert, G. A. & Morris, R. J. Expression of the neuronal surface glycoprotein Thy-1 is under posttranscriptional control, and is spatially regulated, in the developing olfactory system. *Development* **109**, 851–864 (1990).
54. Oueslati, A., Schneider, B. L., Aebischer, P. & Lashuel, H. A. Polo-like kinase 2 regulates selective autophagic  $\alpha$ -synuclein clearance and suppresses its toxicity in vivo. *Proc Natl Acad Sci.* **110**, 3945–3954 (2013).
55. Singleton, A. B. *et al.* alpha-Synuclein locus triplication causes Parkinson's disease. *Science* **302**, 841 (2003).
56. Vekrellis, K. & Stefanis, L. Targeting intracellular and extracellular alpha-synuclein as a therapeutic strategy in Parkinson's disease and other synucleinopathies. *Expert Opin Ther Targets.* **16**, 221–232 (2012).
57. Enwere, E. *et al.* Aging results in reduced epidermal growth factor receptor signaling, diminished olfactory neurogenesis, and deficits in fine olfactory discrimination. *J. Neurosci.* **24**, 8354–8365 (2004).
58. Mandairon, N. *et al.* Neurogenic correlates of an olfactory discrimination task in the adult olfactory bulb. *Eur. J. Neurosci.* **24**, 3578–3588 (2006).
59. Marxreiter, F., Regensburger, M. & Winkler, J. Adult neurogenesis in Parkinson's disease. *Cell Mol Life Sci.* **70**, 459–473 (2013).
60. Fuhrmann, M., Mitteregger, G., Kretzschmar, H. & Herms, J. Dendritic Pathology in Prion Disease Starts at the Synaptic Spine. *J. Neurosci.* **27**, 6224–6233 (2007).

## Acknowledgments

We thank Sonja Steinbach and Eric Griessinger for their excellent technical support and animal care, and Dr. Neville Vassallo for his brilliant suggestions and proofreading. This work was funded by a research fund from EraNetNeuron (01-EW-1006).

## Author contributions

J.N., S.F. and J.H. designed the experiments. S.M. and M.B. provided relevant materials. All authors discussed the results and commented on the manuscript.

## Additional information

**Competing financial interests:** The authors declare no competing financial interests.

**How to cite this article:** Neuner, J., Filser, S., Michalakis, S., Biel, M. & Herms, J. A30P  $\alpha$ -Synuclein interferes with the stable integration of adult-born neurons into the olfactory network. *Sci. Rep.* **4**, 3931; DOI:10.1038/srep03931 (2014).



This work is licensed under a Creative Commons Attribution-NonCommercial-NoDerivs 3.0 Unported license. To view a copy of this license, visit <http://creativecommons.org/licenses/by-nc-nd/3.0>